Interleukin-6 promotes pancreatic cancer cell migration by rapidly activating the small GTPase CDC42

Received for publication, April 3, 2018, and in revised form, May 21, 2018 Published, Papers in Press, May 31, 2018, DOI 10.1074/jbc.RA118.003276

Gina L. Razidlo[‡§1], **Kevin M. Burton**[§¶2], **and Mark A. McNiven**[‡§]

From the [‡]*Division of Gastroenterology and Hepatology,* [§]*Department of Biochemistry and Molecular Biology, and* [¶]*Mayo Clinic Graduate School of Biomedical Sciences, Mayo Clinic, Rochester, Minnesota 55905*

Edited by Alex Toker

Inflammation is a major driver of tumor progression and metastasis, although the mechanisms by which proinflammatory cytokines drive metastatic invasion are unknown. Interleukin-6 (IL-6) is a potent proinflammatory cytokine that is elevated in individuals with pancreatic cancer (PDAC), is required for PDAC progression in mice, and increases tumor cell invasion *in vitro*. Here, we provide insights into the mechanisms by which IL-6 activates tumor cell invasion. We found that IL-6 stimulation rapidly and robustly activates the small GTPase cell division cycle 42 (CDC42) in human PDAC cells and promotes the formation of premigratory filopodia. The CDC42 activation was required for IL-6–induced invasion as blocking CDC42 activity rendered the cells insensitive to IL-6's proinvasive effects. Loss of Janus kinase 2 (JAK2) or signal transducer and activator of transcription 3 (STAT3) prevented IL-6–mediated CDC42 activation, indicating that IL-6 activates CDC42 through both JAK2 and STAT3. However, the rapid activation of CDC42 suggested that this activation may be distinct from canonical STAT3-mediated transcriptional activation. Importantly, we observed an interaction between STAT3 and IQ motif–containing GTPase-activating protein 1 (IQGAP1), a scaffolding platform that binds CDC42. STAT3 colocalized with CDC42 and IQGAP1 at the plasma membrane, suggesting cross-talk between IL-6–mediated STAT3 signaling and CDC42 activation. These results suggest that IL-6 promotes metastatic invasion, at least partially, through CDC42 and that, along with its pleiotropic effects on tumor growth and progression, IL-6 signaling also activates proinvasive GTPase signaling, priming tumor cells for metastatic invasion.

Pancreatic cancer (PDAC)[3] is one of the most lethal forms of human cancer and is the third leading cause of cancer death (1). Evidence suggests that pancreatic cancer is capable of metastatic dissemination very early in its progression (2). Therefore, it is essential to understand the mechanisms by which this early dissemination occurs with the goal of earlier therapeutic intervention to prevent tumor progression and metastasis.

Inflammation is a risk factor for multiple tumor types and is correlated with tumor progression and metastasis *in vitro* and *in vivo* (3). Particularly in pancreatic cancer, the complex tumor microenvironment comprises proinflammatory cells and signals that act to prime the tumor cells and surrounding stroma for metastasis. The pleiotropic inflammatory cytokine interleukin-6 (IL-6) is associated with tumor progression in multiple tumor models and induces diverse cellular effects. IL-6 is abundant in the stroma of pancreatic cancer and is secreted by monocytes and cancer-associated fibroblasts (4–7). *trans*-Signaling from these cell types acts on tumor cells to activate tumor growth and progression (6, 7). Interestingly, IL-6–mediated signaling is required for the early progression of pancreatic cancer (5, 6, 8). In mice that lack IL-6, inflammation- or KRas-driven tumors do not progress beyond the PanIN state. These data indicate that IL-6 is present and acting on tumor cells very early in the development of pancreatic cancer.

IL-6 signaling occurs by IL-6 ligand binding to the IL-6 receptor, a type I transmembrane receptor, coupled with the coreceptor gp130 (9). IL-6 signaling can also occur in *trans* where IL-6 binds to a soluble form of the IL-6 receptor and is still able to bind and activate the coreceptor gp130. Receptor binding triggers autophosphorylation and activation of the Janus kinases (JAKs), which phosphorylate and activate signal transducer and activator of transcription 3 (STAT3) transcription factors, which dimerize, translocate to the nucleus, and bind DNA to regulate transcription. The vast majority of IL-6–dependent effects are due to gene expression changes regulated by the transcriptional regulatory activity of STAT3.

In several tumor models, IL-6 has been shown to increase metastatic capability (9). IL-6 acts on cells in the tumor microenvironment, making it permissive for metastatic dissemination. For example, IL-6 can act on endothelial cells to increase angiogenesis and vascular permeability and can mod-

This work was supported in part by National Institutes of Health Grants R01 CA104125 (to M. A. M. and G. L. R.), P30 DK084567 (Mayo Clinic Center for Cell Signaling in Gastroenterology), and P50 CA102701 (Mayo Clinic Specialized Program of Research Excellence in Pancreatic Cancer (SPORE); to G. L. R.) and the Lustgarden Foundation for Pancreatic Cancer Research. The authors declare that they have no conflicts of interest with the contents of this article. The content is solely the responsibility of the authors and does not necessarily represent the official views of the NCI or the National Institutes of Health.

This article contains Figs. S1–S3 and Movies S1 and S2.

[1] To whom correspondence should be addressed: Mayo Clinic, 200 First St. S. W., Rochester, MN 55905. Tel.: 507-284-0308; Fax: 507-284-2053; E-mail: razidlo.gina@mayo.edu.

[2] Supported by the Mayo Clinic Graduate School of Biomedical Sciences.

[3] The abbreviations used are: PDAC, pancreatic ductal adenocarcinoma; IL-6, interleukin-6; CDC42, cell division cycle 42; JAK, Janus kinase; STAT, signal transducer and activator of transcription; IQGAP1, IQ motif–containing GTPase-activating protein 1; PanIN, pancreatic intraepithelial neoplasia; EMT, epithelial-to-mesenchymal transition; PDGF, platelet-derived growth factor; PBD, p21-binding domain; GEF, guanine nucleotide exchange factor; ERK, extracellular signal-regulated kinase; DMEM, Dulbecco's modified Eagle's medium; EGF, epidermal growth factor; GST, glutathione *S*-transferase; RBD, RhoA-binding domain.

© 2018 Razidlo et al. Published under exclusive license by The American Society for Biochemistry and Molecular Biology, Inc.
This is an Open Access article under the CC BY license.

ulate the immune environment in tumors (9). IL-6 signaling also up-regulates the secretion of matrix-degrading metalloproteinases, including MMP7 (10). IL-6 also acts directly on tumor cells to promote survival and invasive migration. The best described mechanism by which IL-6 increases migration of tumor cells is by conferring an "epithelial-to-mesenchymal transition" (EMT) phenotype to tumor cells through the up-regulation of EMT marker genes, including Snail and Twist (11). Although an EMT gene expression pattern has been well-correlated with increased tumor cell migration, there is also recent controversy in the role of EMT in metastasis (12–14). In recent studies, removal of the classic EMT factor Twist does not actually suppress metastasis in mouse models of pancreatic cancer (14). It is likely that disseminating tumor cells use EMT-dependent and EMT-independent mechanisms of invasive migration. Thus, IL-6 may also up-regulate metastatic invasion via EMT-independent pathways.

Invasive cell migration is regulated by the Rho family of small GTPases, including RAC1 and CDC42, which activate downstream effectors to induce actin cytoskeletal remodeling (15). RAC1 and CDC42 regulate actin polymerization and branching that drive the formation of lamellipodia and filopodia, respectively, which are actin-based structures that are mechanical drivers of cell protrusion and migration. These GTPases act at the plasma membrane and cycle between an active, GTP-bound state and an inactive, GDP-bound state. The activity of the GTPases is controlled by a host of regulatory proteins, many of which are dysregulated in cancers. It is unclear how IL-6 may interact with the RhoGTPases in pancreatic cancer cells to regulate promigratory signaling pathways.

In this study, we investigated the molecular mechanisms by which IL-6 acts directly on tumor cells to increase invasive migration. Here, we present data that IL-6 promotes pancreatic tumor cell migration, at least in part, through rapid activation of the GTPase CDC42. Thus, we propose a novel role for the canonical IL-6 signaling pathway in supporting metastatic dissemination in pancreatic cancer cells.

Results

Interleukin-6 induces invasive cell migration in pancreatic cancer cells

To investigate the effects of IL-6 on tumor cell invasion, pancreatic cancer cells were treated with IL-6, and their invasive properties were quantified in cell culture. PANC-1 pancreatic cancer cells were seeded in a chemotactic transwell migration assay in the presence or absence of IL-6 (0–100 ng/ml) for 7 h. The presence of IL-6 significantly increased the invasive potential of the tumor cells and caused a 3-fold increase in transwell migration rate (Fig. 1*A*). IL-6 induced transwell migration to a level comparable with that of a positive control, PDGF (30 ng/ml). This effect was specifically due to IL-6 signaling as treatment of cells with blocking antibodies to the IL-6 receptor or the coreceptor gp130 blocked the promigratory effects of IL-6 (Fig. 1*A*). IL-6 also activated transwell migration in CFPAC pancreatic cancer cells and in two pancreatic cancer cells derived from human tumors and cultured as patient-derived xenografts (5160-1 and 6741-1 (16); Fig. S1, *A–C*).

In addition, when seeded in a wound healing assay, the presence of IL-6 enhanced tumor cell migration of PANC-1 cells in either the presence or absence of serum (Fig. 1*B*). Thus, IL-6 increases the migratory potential of pancreatic cancer cells.

It has previously been shown that IL-6 can increase cancer cell proliferation. Therefore, we tested whether the promigratory effects observed were actually an effect on tumor cell proliferation. However, under the acute experimental time points used, IL-6 was not sufficient to increase cell proliferation. Whereas the migration assays were performed after 7–24 h in the absence of serum, IL-6 only led to increased proliferation after at least 3 days of treatment and only in the presence of serum (Fig. S1*D*). Therefore, the promigratory effects of IL-6 are unlikely to be due to increased proliferation.

Therefore, we sought to determine whether IL-6 signaling acted acutely on the invasive cellular machinery to promote migration. To this end, pancreatic cancer cells were transfected with GFP-actin. This approach allows the monitoring of cytoskeletal and morphological changes following IL-6 stimulation using live-cell fluorescence microscopy. PANC-1 cells were cultured in the absence of serum overnight and then stimulated with IL-6 (50 ng/ml). Within minutes of IL-6 addition, changes were apparent in the cell shape and actin distribution (Fig. 1*C*, Fig. S1*E*, and Movies S1 and S2). Kymography revealed remodeling of GFP-actin at the cell periphery and the formation of protrusions. The ImageJ plugin FiloQuant was used to quantify the presence of filopodia before and after IL-6 stimulation (17). IL-6 treatment resulted in a significant 60% increase in the number of filopodia within 30 min (Fig. 1*D*). Thus, IL-6 treatment induces formation of filopodia and invasive cell migration in pancreatic cancer cells.

IL-6 stimulates rapid activation of CDC42

The canonical formation of filopodia is attributed to signaling through the Rho family GTPase CDC42. Therefore, we tested whether IL-6 treatment led to the activation of CDC42. This was accomplished by a biochemical pulldown using the p21-binding domain (PBD) of the RAC/CDC42 effector PAK1 fused to glutathione *S*-transferase (GST-PBD). PANC-1 cells were grown in serum-free medium overnight and then stimulated with IL-6 (50 ng/ml) for 0–60 min. Strikingly, IL-6 stimulation led to rapid and sustained activation of CDC42 (Fig. 2*A*). CDC42 was activated within 5 min of IL-6 treatment and remained activated after 1 h. A dose-response curve demonstrated that IL-6 activated CDC42 from 1 to 50 ng/ml to a level comparable with the positive control, 10% FBS (Fig. S2*A*). In contrast, IL-6 did not activate the related GTPases RAC1 or RhoA, indicating specificity for CDC42 (Fig. 2, *B* and *C*). Similar results were observed in the CFPAC pancreatic cancer cell line (Fig. S2, *B* and *C*) where IL-6 stimulation rapidly activated CDC42 within minutes but had no effect on RAC1 activation. IL-6–mediated activation of CDC42 was also observed in 5160-1 and 6741-1 human pancreatic cancer cells as well as the established cell lines MiaPaCa2 and Panc.0403 (Fig. S2, *D–G*). This activation of CDC42, but not RAC1, is consistent with the morphological changes described in Fig. 1*C* where IL-6 promotes formation of CDC42-dependent filopodia but not RAC-dependent lamellipodia.

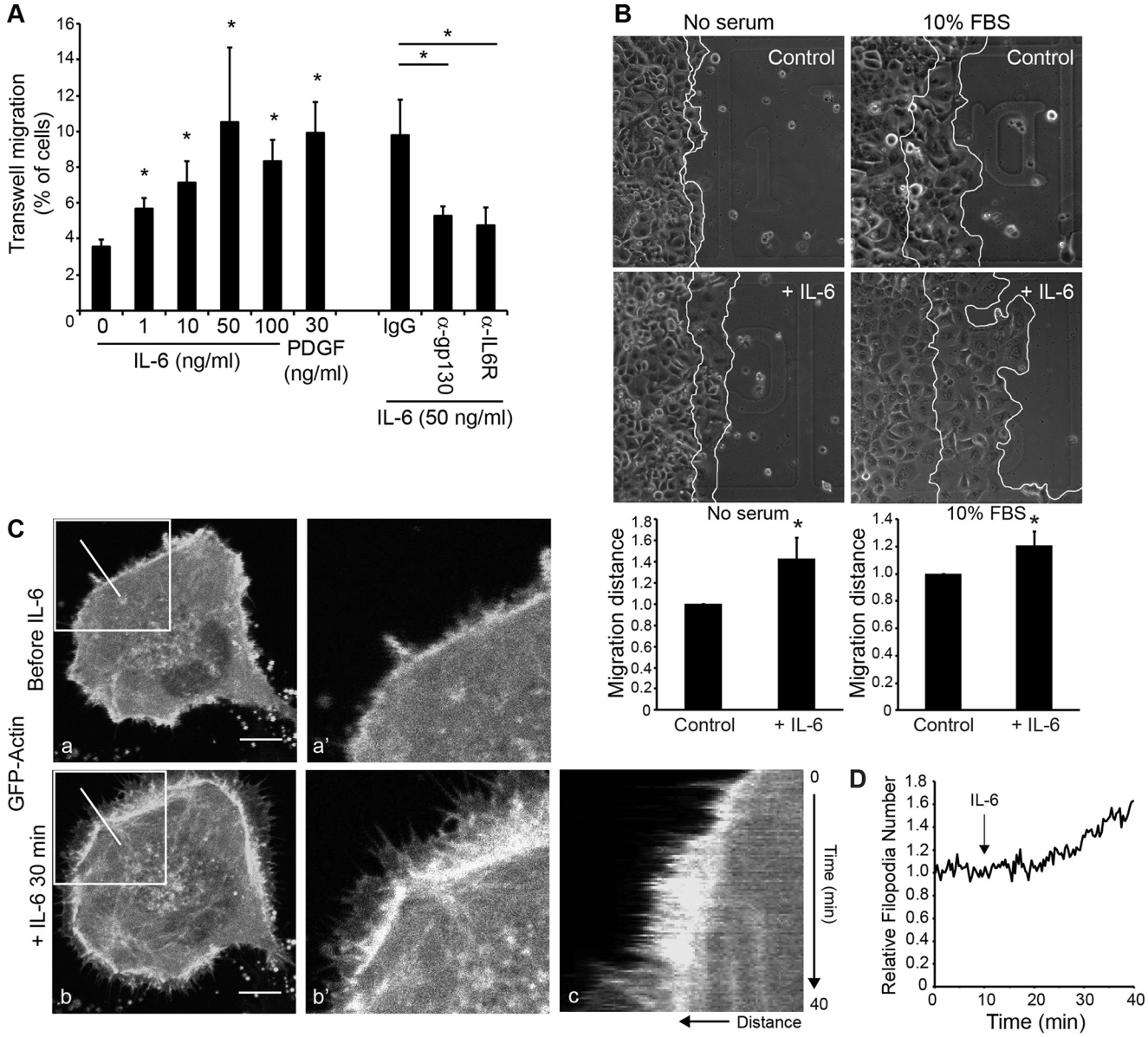

Figure 1. IL-6 promotes migration of pancreatic cancer cells. *A*, PANC-1 cells were plated in a chemotactic transwell migration assay in the presence or absence of IL-6 (0–100 ng/ml) for 7 h. PDGF (30 ng/ml) was used as a positive control. As a specificity control, cells were incubated with blocking antibodies to IL-6 receptor (*IL6R*) or the coreceptor gp130, compared with IgG control, in the presence of IL-6 (50 ng/ml). The percentage of cells that migrated across a transwell filter is shown. Graphed data represent the mean of three to five independent experiments. *Error bars* represent S.E. * indicates $p < 0.05$. *B*, migration of PANC-1 cells was measured by a wound healing assay. Representative images show PANC-1 cells before and after wounding a confluent monolayer in the absence of serum (*left*) or presence of 10% FBS (*right*) ±IL-6 (50 ng/ml). *White lines* indicate the starting ($t = 0$ h) and ending edges of the migrating cells ($t =$ 24 h for no serum and 16 h for 10% FBS). Graphed data indicate the relative distance migrated, normalized to control cells. *C*, IL-6 induces filopodial actin protrusions. PANC-1 cells were transfected to express GFP-actin and then imaged using live-cell fluorescence microscopy while stimulated with IL-6 (50 ng/ml). *Panel a* represents a cell prior to IL-6 addition, and *panel b* represents the same cell 30 min after IL-6 addition. *Boxed* regions are magnified at *right* (*panels a'* and *b'*). *Panel c* represents a kymograph from the region denoted with a *white line*. *Scale bars*, 10 μm. *D*, the number of filopodia was measured using live-cell imaging from eight cells from independent biological replicates using the FiloQuant program in ImageJ. The basal number of filopodia was set to 1 for each cell, and the graph represents the average relative number of filopodia following addition of IL-6. See also Fig. S1 and Movies S1 and S2.

We next sought to determine whether IL-6–mediated CDC42 activation contributed to the proinvasive and migratory effects of IL-6. First, CDC42 was depleted by transfection of siRNA into PANC-1 cells, which were then seeded in a chemotactic transwell migration assay in the presence or absence of IL-6. As observed previously, IL-6 treatment increased the invasive migration of the control tumor cells. However, in the absence of CDC42, IL-6 was no longer able to stimulate transwell migration, demonstrating that CDC42 is required for IL-6–induced migration (Fig. 3*A*). The same results were observed using two independent siRNAs, the knockdown efficiencies of which are shown in Western blots from parallel samples used in Fig. 3*C*. As an additional approach, PANC-1 cells were transfected with a dominant-negative form of CDC42 T17N or control vector, and the cells were seeded in a transwell assay in the presence or absence of IL-6. Cells expressing CDC42 T17N were identified by immunostaining for the expressed construct. Consistent with the data in Fig. 3*A*, IL-6 stimulation increased transwell migration in the control cells, but this was impaired in cells expressing dominant-negative

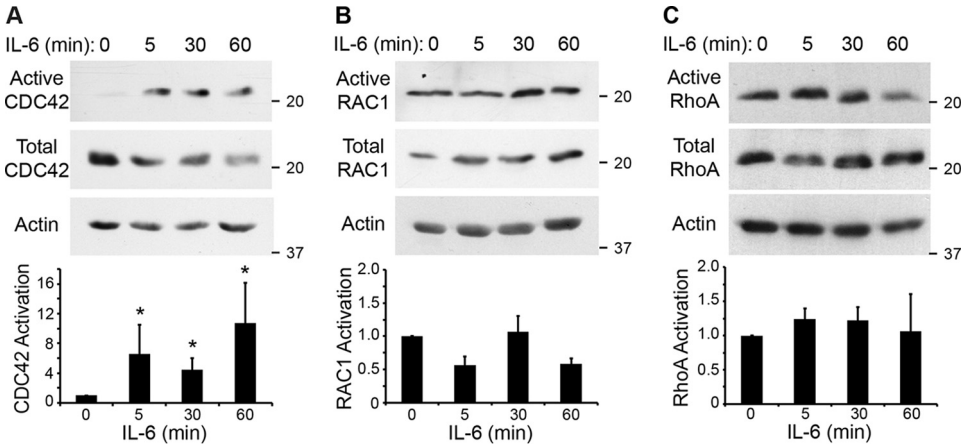

Figure 2. IL-6 stimulation leads to activation of CDC42 in pancreatic cancer cells. *A*, IL-6 rapidly activates CDC42. PANC-1 cells were treated with IL-6 for the indicated times (50 ng/ml), then lysed, and analyzed for CDC42 activation using a GST-PBD biochemical pulldown and Western blotting for CDC42. Note the rapid and robust activation of CDC42 within just 5 min post-stimulation. Active CDC42 was normalized to total CDC42 and compared with the ratio at $t = 0$. *B*, in contrast, IL-6 stimulation did not activate RAC1. PANC-1 cells were treated as described in *A*, and active RAC1 was precipitated using a GST-PBD pulldown followed by Western blotting for RAC1. Active RAC1 was normalized to total RAC1 and compared with the ratio at $t = 0$. *C*, IL-6 does not significantly activate RhoA. PANC-1 cells were stimulated with IL-6 as above, and active RhoA was precipitated using a GST-RBD pulldown followed by Western blotting for RhoA. Active RhoA was normalized to total RhoA and compared with the ratio at $t = 0$. Relative levels of RAC1, CDC42, or RhoA activation are graphed as the mean of three to six independent biological replicates. *Error bars* represent S.E. * indicates $p < 0.05$. See also Fig. S2.

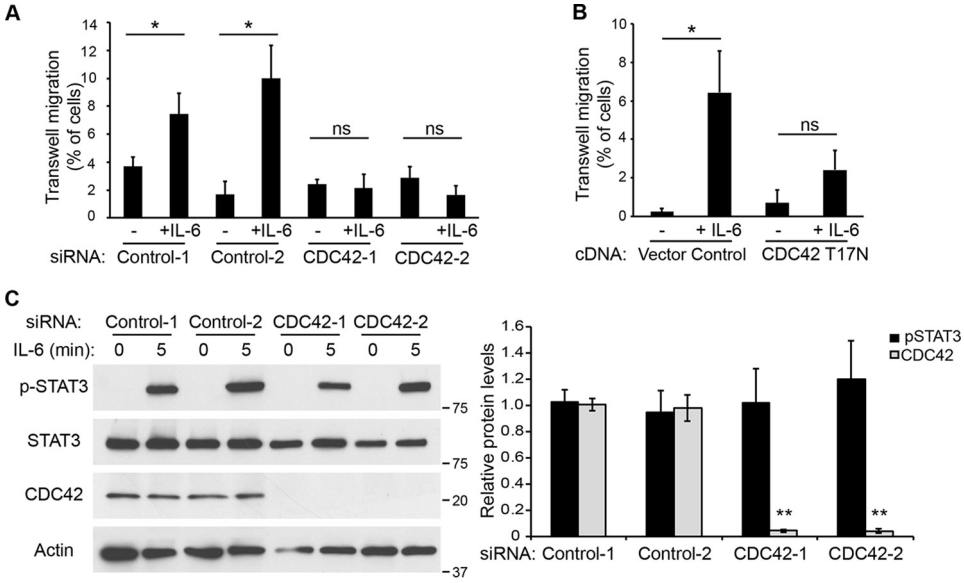

Figure 3. CDC42 activation is required for IL-6 to promote invasive cell migration. *A*, RNAi-mediated knockdown of CDC42 prevents IL-6–induced transwell migration. PANC-1 cells were transfected with nontargeting control siRNAs or siRNAs targeting CDC42. Cells were seeded in a chemotactic transwell migration assay in the presence or absence of IL-6 (50 ng/ml) for 7 h. The percentage of cells that migrated across a gelatin-coated transwell filter is shown. Knockdown efficiency of CDC42 was confirmed in samples transfected in parallel and is shown in *C*. *B*, overexpression of dominant-negative CDC42 T17N prevents IL-6–induced transwell migration. PANC-1 cells were transfected with an empty vector or myc-tagged CDC42 T17N. Cells were seeded in a chemotactic transwell migration assay as described in *A*, then fixed, and stained for myc-CDC42 T17N overexpression. Only cells positive for the transfected construct were scored for the CDC42 T17N condition. The percentage of cells that migrated across a gelatin-coated transwell filter is shown. *C*, CDC42 is not required for IL-6 to activate STAT3. PANC-1 cells were depleted of CDC42 using the indicated siRNAs and stimulated with IL-6 (50 ng/ml) for 5 min, and STAT3 phosphorylation was assayed by Western blotting. STAT3 was still phosphorylated in the absence of CDC42. Graphed data represent both phosphorylated STAT3 (*p-STAT3*) and CDC42 protein levels following siRNA-mediated knockdown. For *A*–*C*, graphed data represent the mean of three to six independent biological replicates. *Error bars* represent S.E. *, $p < 0.05$; **, $p < 0.01$; *ns*, not a statistically significant difference.

CDC42 (Fig. 3*B*). These data indicate that CDC42 activity is required for IL-6 to promote invasive migration and suggest that IL-6 regulates tumor cell invasion, at least in part, through activation of CDC42.

It is possible that CDC42 activation is upstream of IL-6–mediated STAT3 activation and thus loss of CDC42 simply inhibits all STAT3-dependent functions, including transcriptional changes that may lead to invasive migration. To test this, we assessed whether CDC42 was required for IL-6 to activate STAT3 as measured by phosphorylation. CDC42 was depleted in PANC-1 cells by siRNA, the cells were stimulated with IL-6 (50 ng/ml; 5 min), and STAT3 phosphorylation was assessed by immunoblotting. As expected, IL-6 induced a robust phosphorylation of STAT3 within 5 min, demonstrating its activation. Importantly, STAT3 phosphorylation was just as robust in the absence of CDC42 (Fig. 3*C*). Similar results were observed using two independent siRNAs. These data indicate that CDC42 is not required for STAT3 phosphorylation and activa-

tion. Therefore, the migration defects observed in Fig. 3, *A* and *B*, are not simply a consequence of impaired STAT3 function. Importantly, these data also show that loss of CDC42 prevented IL-6–dependent invasion even in the presence of activated STAT3. STAT3 is phosphorylated in the absence of CDC42; however, IL-6 is not able to promote invasive transwell migration (Fig. 3, *A* and *C*). This suggests that IL-6–mediated CDC42 activation promotes tumor cell migration by a pathway distinct from canonical STAT3 signaling.

The IL-6 effectors JAK2 and STAT3 are required for CDC42 activation

It was intriguing that IL-6 activates CDC42 within minutes, which appeared to be too rapid to be a consequence of STAT3-dependent transcription. Therefore, we investigated the mechanisms by which the IL-6 signaling pathway could cross-talk with the CDC42 pathway. IL-6 binding to its receptor and coreceptor induces the activation of the kinase JAK. Therefore, we tested whether JAK was required for IL-6 to activate CDC42. JAK2 was depleted in PANC-1 cells by siRNAs, the cells were stimulated with IL-6 (50 ng/ml; 5 min), and CDC42 activation was assessed by GST-PBD pulldown and immunoblotting. In control cells, IL-6 stimulated CDC42 activation by 2-fold, consistent with our previous observations. However, IL-6 stimulation was unable to activate CDC42 in the absence of JAK2 (Fig. 4*A* and Fig. S3, *A* and *B*). Similar results were obtained using two independent siRNAs for JAK2. These data suggest that JAK2 is required for the IL-6 pathway to cross-talk with the CDC42 activation pathway. In leukocytes and some cancer cells, JAKs can phosphorylate GEFs to promote activation of RAC, including VAV1 and VAV2 (18, 19). As these GEFs also have activity toward CDC42, we hypothesized that JAK2 could similarly signal through the VAV proteins in pancreatic cancer cells. However, VAV1 is not expressed in PANC-1 cells, and VAV2 phosphorylation is not induced following IL-6 stimulation (data not shown). This led us to hypothesize that there is a novel mechanism of cross-talk between these two potent signaling pathways.

We next tested whether the JAK2 substrate STAT3 is required for CDC42 activation. PANC-1 cells were transfected with a control siRNA or siRNAs targeting STAT3, and the cells were stimulated with IL-6 (50 ng/ml; 5 min). In the control cells, IL-6 promoted CDC42 activation. However, this increase was blocked in cells depleted of STAT3, suggesting that STAT3 is required for IL-6 to activate CDC42 (Fig. 4*B* and Fig. S3, *A[R] and C*). Similar results were obtained using two independent siRNAs for STAT3. As an additional approach, PANC-1 cells were treated with the STAT3 inhibitor S3I-201, which is described to inhibit STAT3 dimerization, phosphorylation, and DNA binding (20). PANC-1 cells were treated with DMSO vehicle control or with S3I-201 for 1 h and then stimulated with IL-6 (50 ng/ml) for 5 min. Again, in the control cells, IL-6 led to activation of CDC42, but this activation was blocked in the presence of the STAT3 inhibitor (Fig. 4*C*). Finally, a dominant-negative mutation of STAT3 was tested for its ability to activate CDC42. Mutation of the activating phosphorylation site Tyr-705 (Y705F) results in a form of STAT3 that cannot be phosphorylated and activated and that appears to have additional

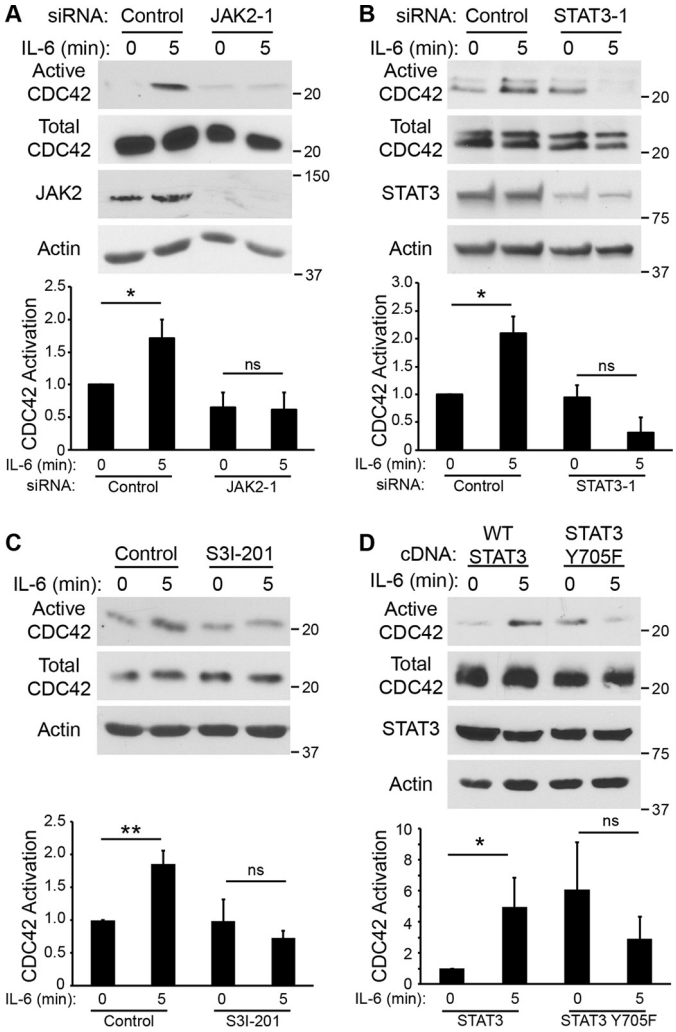

Figure 4. JAK/STAT signaling is required for IL-6 to activate CDC42. *A*, knockdown of JAK2 prevents IL-6 from activating CDC42. PANC-1 cells were transfected with a control nontargeting siRNA or an siRNA against JAK2 and then stimulated with IL-6 (50 ng/ml) for 5 min. Active CDC42 was precipitated using a GST-PBD biochemical pulldown and Western blotting for CDC42. *B*, knockdown of STAT3 prevents IL-6 from activating CDC42. PANC-1 cells were transfected with a control nontargeting siRNA or an siRNA against STAT3 and then treated as described in *A*. *C*, PANC-1 cells were treated with DMSO vehicle control or the STAT inhibitor S3I-201 (100 μM) for 1 h and then treated with IL-6 (50 ng/ml) for 5 min, and CDC42 activity was assessed as described above. *D*, a dominant-negative STAT3 mutant prevents activation of CDC42 by IL-6. PANC-1 cells were transfected to overexpress WT STAT3 or STAT3 Y705F and then treated with IL-6 (50 ng/ml; 5 min). CDC42 activation was assessed as described above. In *B–D*, IL-6 stimulation led to activation of CDC42 but not following inhibition of STAT3 using RNAi, a chemical inhibitor, or a phosphomutant. For *A–D*, active CDC42 was normalized to total CDC42, and the ratios were compared with $t = 0$ in the control cells. Data are represented as the mean of three to five independent biological replicates. *Error bars* represent S.E. *, $p < 0.05$; **, $p < 0.01$; *ns*, not a statistically significant difference. See also Fig. S3.

dominant-negative effects on dimerization (21). PANC-1 cells were transfected with WT STAT3 or STAT3 Y705F, and CDC42 activity was assessed by GST-PBD pulldown. As expected, IL-6 promoted activation of CDC42 in the control, STAT3-expressing cells. In cells expressing dominant-negative STAT3 Y705F, basal levels of CDC42 activity were elevated, but IL-6 treatment was unable to stimulate an increase in CDC42 activity (Fig. 4*D*). Thus, using multiple approaches, loss of STAT3 function prevented IL-6–dependent activation of

CDC42, suggesting that STAT3 is required for the IL-6 pathway to cross-talk to the CDC42 pathway.

IQGAP1 mediates the cross-talk between STAT3 and CDC42

The vast majority of IL-6–mediated STAT3 functional effects are attributed to STAT3 transcriptional activity, which depends on its phosphorylation and dimerization. The data in Fig. 4 suggest that STAT3 is required for IL-6 to activate CDC42. However, the extremely rapid activation of CDC42 within minutes of IL-6 stimulation suggests that this response is too early to be an effect of STAT-mediated transcription. Transcription-independent functions of STAT3 have been described, including via protein–protein interactions (22–24), which may be regulated by STAT3 phosphorylation and/or dimerization. Therefore, we hypothesized that STAT3 could bind a cytoplasmic protein that could mediate the cross-talk between the STAT3 and CDC42 signaling pathways. To this end, we sought to identify novel cytoplasmic binding partners of STAT3 by MS.

Cytoplasmic fractions were prepared from PANC-1 cells; STAT3 was immunoprecipitated; and STAT3-associated proteins were resolved by SDS-PAGE, silver staining, and MS. Using this approach, IQGAP1 was identified as a novel interacting partner of STAT3. IQGAP1 is a scaffold protein that binds to CDC42 to regulate its activation and thus represented an exciting candidate that could link STAT3 to CDC42. Importantly, IQGAP1 also integrates multiple signaling pathways through interactions with numerous proteins, including ERK, actin, β-catenin, calmodulin, and others (25, 26). Therefore, IQGAP1 could represent an important mechanism to integrate IL-6 signaling with multiple cellular signaling pathways, including CDC42. First, an interaction between STAT3 and IQGAP1 was confirmed by immunoprecipitation. Endogenous STAT3 was immunoprecipitated from PANC-1 cells, and immunoblotting revealed that endogenous IQGAP1 does associate with STAT3 (Fig. 5*A*).

We predicted that STAT3 might colocalize with the IQGAP1–CDC42 activation complex, potentially at the cell periphery, where CDC42 would be activated to remodel the actin cytoskeleton. PANC-1 cells were transfected with GFP-CDC42 and then immunostained for endogenous STAT3 and IQGAP1 in the presence or absence of IL-6. Indeed, in a subset of cells, STAT3 could be found colocalized at the plasma membrane with IQGAP1 and CDC42. Even upon stimulation with IL-6, whereupon there was a translocation of STAT3 to the nucleus, there remained a fraction of STAT3 associated with the plasma membrane in about 30% of cells (Fig. 5*B*). These data support the biochemical data showing an association between IQGAP1 and CDC42,

If IQGAP1 links IL-6 signaling to CDC42, we predicted that loss of IQGAP1 would inhibit the ability of IL-6 to activate CDC42. PANC-1 cells were depleted of IQGAP1 using siRNA and were stimulated with IL-6, and CDC42 activation was assayed using a GST-PBD pulldown. In control cells, IL-6 stimulated CDC42 activation as observed previously (Fig. 5*C*). In IQGAP1-depleted cells, basal levels of CDC42 activation were elevated, but the IL-6–dependent stimulation of CDC42 was blocked. These data suggest that IQGAP1 is required for IL-6 to activate CDC42. Finally, we predicted that IQGAP1 would also be required for IL-6 to stimulate invasive transwell migration. PANC-1 cells were depleted of IQGAP1 using siRNA, and then the cells were seeded in a transwell migration assay in the presence or absence of IL-6. IL-6 stimulated the transwell migration of control PANC-1 cells as expected. However, this promigratory effect of IL-6 was inhibited in the absence of IQGAP1 (Fig. 5, *D* and *E*). These data are consistent with the requirement for IQGAP1 in IL-6–mediated CDC42 activation and promigratory signaling. Thus, we propose a model whereby the scaffold protein IQGAP1 serves as a platform to coordinate signaling between IL-6–mediated STAT3 activation and CDC42-dependent actin remodeling and invasive migration (Fig. 5*F*).

Discussion

Inflammation is associated with cancer progression and metastasis in multiple tumor types. The data presented here define a novel mechanism by which the inflammatory cytokine IL-6 can act directly on tumor cells to up-regulate the migratory machinery via activation of CDC42. This requires signaling through the canonical IL-6 effectors JAK2 and STAT3. Due to the rapid activation of CDC42 within minutes of IL-6 stimulation, it is unlikely that CDC42 activation is the consequence of STAT3-dependent transcription. Instead, we have uncovered a novel interaction between STAT3 and the scaffolding protein IQGAP1, which is known to bind CDC42 and coordinate cell migration (25, 27). We propose that this IQGAP1 signaling platform can couple signals from the IL-6 pathway to the CDC42 pathway.

Indeed, IQGAP1 likely integrates signals from multiple stimuli to serve as a hub for cross-talk among potent cellular signaling pathways (26). In addition to binding CDC42 and several of its regulators, IQGAP1 also interacts with RAC, Rho, and actin to regulate cytoskeletal dynamics and migration. IQGAP1 also binds and coordinates signaling through the mitogen-activated protein kinase pathway; components of the Akt signaling pathway; adhesion proteins, including N-cadherin and integrins; the Wnt pathway; and scaffolding proteins for other pathways. Furthermore, IQGAP1 can coordinate with multiple receptors, allowing it to integrate stimuli and facilitate signal transduction (for a review, see Ref. 26). The association between STAT3 and IQGAP1 may be direct or may be indirect through one of the many IQGAP1-binding partners. Interestingly, a mutated version of JAK associated with a myeloproliferative disorder results in aberrant IQGAP1 expression, although the mechanisms of this dysregulation are unclear (28). Thus, in addition to CDC42-dependent migration, an association between IQGAP1 and STAT3 could bridge cytokine-induced STAT3 activation with multiple potent cellular signaling pathways.

Although IQGAP1 is a binding partner of CDC42 and has been proposed to enhance CDC42 activity (25), the specific mechanism by which CDC42 is activated following IL-6 stimulation remains to be determined. IL-6–mediated activation of CDC42 should require the activity of a GEF or the inhibition of a GTPase-activating protein or guanine nucleotide dissociation inhibitor. Along this line, JAK signaling has been described to phosphorylate and activate a subset of GEFs for RAC and Rho (18, 29). In addition, STAT3 has been described to bind the GEF

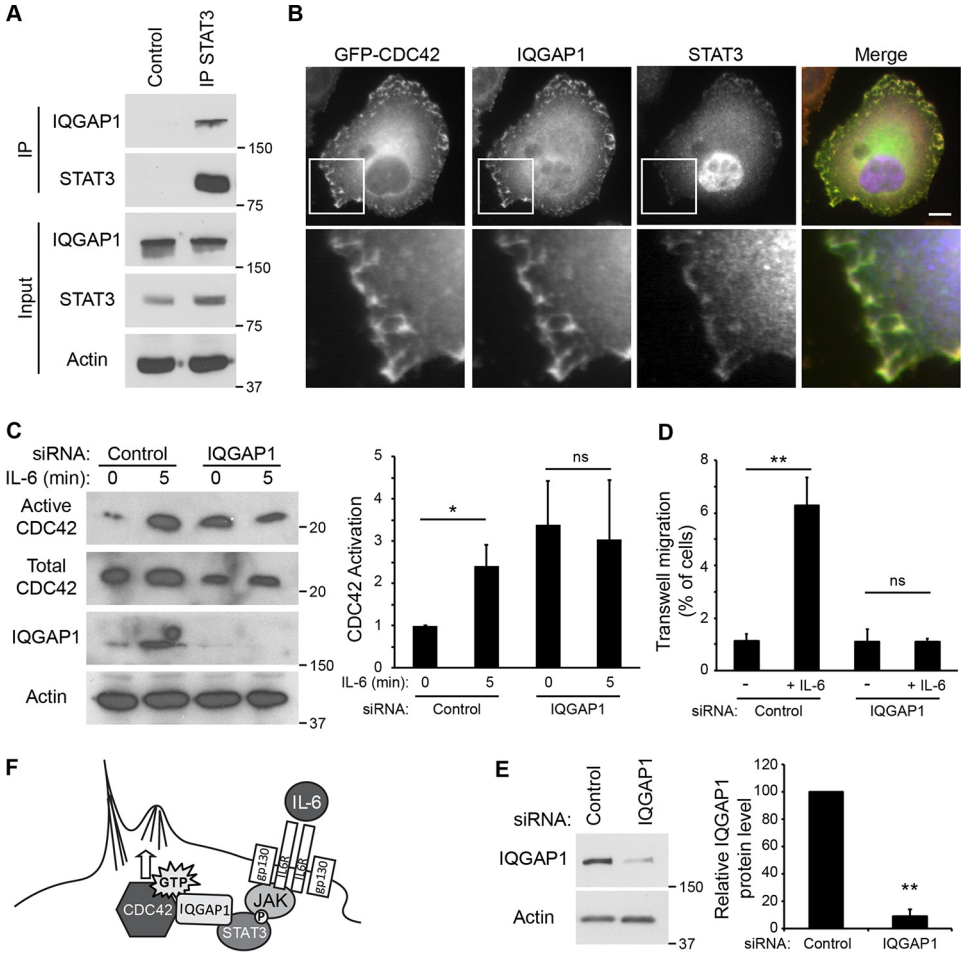

Figure 5. STAT3 associates with the CDC42 adaptor IQGAP1. *A*, IQGAP1 coimmunoprecipitates with STAT3. Lysates from PANC-1 cells treated with IL-6 (50 ng/ml; 5 min) were immunoprecipitated (*IP*) for STAT3 or incubated with Protein A beads alone as a control, and STAT3 and IQGAP1 were detected by immunoblotting. A lower exposure was used for the IQGAP1 input blot to demonstrate equal protein loading. *B*, STAT3 colocalizes at the plasma membrane with CDC42 and IQGAP1. PANC-1 cells were transfected with GFP-CDC42, treated with IL-6 (50 ng/ml; 5 min), then immunostained for endogenous STAT3 and IQGAP1. In a subset of cells, STAT3 can be found enriched near the plasma membrane, colocalized with GFP-CDC42 and IQGAP1. *Scale bar*, 10 μm. *C*, IQGAP1 is required for IL-6 to activate CDC42. PANC-1 cells were transfected with a control nontargeting siRNA or an siRNA targeting IQGAP1 and treated with IL-6 (50 ng/ml), and then CDC42 activation was assessed by GST-PBD pulldown. Active CDC42 was normalized to total CDC42 and compared with untreated control cells in each experiment. *D*, IQGAP1 is required for IL-6 to promote transwell migration. PANC-1 cells were transfected with a control nontargeting siRNA or an siRNA targeting IQGAP1 and then seeded in a transwell assay in the presence or absence of IL-6 (50 ng/ml) for 7 h. The percentage of cells that migrated across a gelatin-coated filter is shown. *E*, representative Western blot demonstrating siRNA-mediated knockdown of IQGAP1 in *D*. Graphed data represent relative levels of IQGAP1 following knockdown, normalized to actin and compared with control nontargeting siRNA. Graphed data represent the mean of three to four independent biological replicates. *Error bars* represent S.E. *, $p < 0.05$; **, $p < 0.01$; *ns*, not a statistically significant difference. *F*, model showing that IQGAP1 links IL-6 stimulation to CDC42 signaling.

β-PIX (PAK-interacting exchange factor β) and negatively regulate RAC activation in fibroblasts (24). Although we were unable to detect these specific effects in pancreatic cancer cells, it is likely that CDC42-regulatory proteins are recruited to the STAT3/IQGAP1–containing complex, potentially regulated by IL-6–mediated STAT3 phosphorylation.

Intriguingly, basal levels of CDC42 activity are elevated following select manipulations of the STAT3/IQGAP1 pathway (Figs. 4*D* and 5*C*). This may suggest that the JAK/STAT pathway negatively regulates CDC42 activation, perhaps via cross-talk with another pathway or through transcriptional regulation of other factors. Even so, this elevated basal activity of CDC42 was not sufficient to induce transwell migration. When PANC-1 cells were depleted of IQGAP1, they exhibited elevated basal CDC42 activity (Fig. 5*C*), but this did not translate to elevated transwell migration (Fig. 5, *D* and *E*). This suggests that other factors are also required for coordinating IL-6–induced CDC42 activation with invasive migration, such as proper targeting or localization of CDC42. Independent of the basal levels of CDC42 activity, inhibition of STAT3, JAK2, or IQGAP1 all prevented the acute IL-6–mediated increase in CDC42 activation.

In pancreatic cancers, IL-6 is a potent activator of multiple aspects of tumor growth and progression. It was previously proposed that IL-6 promoted invasive migration through induction of an EMT program, regulated by STAT3-mediated transcription. Here, we propose that IL-6 can also act more acutely to regulate cytoskeletal dynamics and migration in tumor cells through activation of CDC42. Interestingly, IL-6 was able to stimulate CDC42 activation in cell types that exhibited a mesenchymal morphology and markers (MiaPaCa2, 5160-1, and 6174-1) as well as those with more epithelial characteristics (Panc04.03). This suggests that, beyond induction of EMT, IL-6 can act on tumor cells in the presence or absence of an EMT

signature to increase migratory potential. Thus, IL-6 can likely activate tumor cell migration by multiple mechanisms, including CDC42 activation and the previously reported EMT gene expression.

IL-6 is likely expressed by multiple cellular sources within the pancreatic tumor microenvironment, including myeloid cells, cancer-associated fibroblasts, and tumor cells (4–6). Inhibition of IL-6 action prevents PanIN formation or progression to PDAC in mouse models (5, 6), demonstrating that it is present and active very early in PDAC development. Importantly, this stage of early lesion development may also provide the window where metastatic dissemination begins. Lineage tracing mouse models revealed that disseminated pancreatic cells are found in the circulation and liver when pancreatic lesions were still in the PanIN stage (2). These data challenged the dogma that cancer cell invasion only occurs at late stages of tumor development, and they also demonstrate dissemination occurring in a window when IL-6 is known to be acting on pancreatic tumor cells. Our findings integrate these two concepts and suggest that IL-6 present at early stages in pancreatic tumor progression may prime tumor cells for dissemination through activation of CDC42. In addition to the formation of filopodia, CDC42 activation is also implicated in polarized migration and the formation of matrix-degrading invadopodia (15). Thus, elevated CDC42 activity has the potential to act in multiple capacities to stimulate cancer cell invasion.

It is important to note that IL-6–mediated activation of CDC42 was not universal in all cell lines tested. In DanG pancreatic cancer cells, IL-6 treatment stimulated STAT3 phosphorylation but did not lead to activation of CDC42 and did not stimulate transwell migration. Due to the heterogeneity among tumor cell lines, it is likely that specific factors downstream of the IL-6 receptor may be differentially expressed or regulated in different tumor cells. This is directly comparable with heterogeneity among patient tumors. As such, it is important to establish specific biomarkers to stratify patient outcomes and responsiveness to certain therapeutic approaches and to treat patients depending on the molecular signature of their tumors. This could be important for patients with inflammation-driven tumors to determine which might be most susceptible to IL-6–mediated metastatic invasion.

Experimental procedures

Cell culture and reagents

PANC-1 human pancreatic cancer cells were obtained from ATCC (CRL-1469). CFPAC, MiaPaCa2, and Panc.0403 human pancreatic cancer cells were provided by Dr. Dan Billadeau, Mayo Clinic. PANC-1, CFPAC, and MiaPaCa2 cell lines were maintained in DMEM + 10% FBS in the presence of penicillin and streptomycin. Panc04.03 cells were maintained in RPMI 1640 medium + 10% FBS in the presence of penicillin and streptomycin. Human pancreatic cancer cells 5160-1 and 6741-1, provided by the Mayo Clinic SPORE, were derived from human tumors that were cultured as patient-derived xenografts as described previously (16) and maintained in DMEM/F-12 + 10% FBS in the presence of penicillin and streptomycin. All tissues were obtained and used in accordance with the Mayo Clinic Institutional Review Board and abide by the Declaration of Helsinki principles. Cells were screened for *Mycoplasma* contamination by PCR (Southern Biotech) or DAPI staining. IL-6 was purchased from Peprotech (200-06) and used at 0–100 ng/ml for the indicated times. PDGF (Peprotech) was used at 30 ng/ml, and EGF (Sigma) was used at 30 ng/ml. S3I-201 (Selleckchem, S1155) was resuspended in DMSO and used at 100 μM for 1 h prior to IL-6 treatment.

cDNA and RNAi transfections

Plasmid cDNAs were transfected using Lipofectamine 2000 (Invitrogen) according to the manufacturer's instructions. pRK5-myc-CDC42-T17N was a gift from Dr. Gary Bokoch (Addgene plasmid 12973). pcDNA3-STAT3 and pcDNA3-STAT3 Y705F-FLAG were gifts from Dr. Jie Chen (Addgene plasmids 74433 and 74434) (30). pcDNA3-STAT3-FLAG was generated by site-directed mutagenesis by reverting the Y705F mutation to WT using primers 5′-CCAGGTAGTGCTGCCCCGTACCTGAAGACCAAGTTC-3′ (forward) and 5′-GAACTTGGTCTTCAGGTACGGGGCAGCACTACCTGG-3′ (reverse), which also reversed a silent AfeI restriction enzyme site. Mouse β-actin in the pEGFP-C2 vector was provided by Dr. Gerald Marriott (31).

RNAi transfections were performed using Lipofectamine RNAiMAX (Invitrogen) according to the manufacturer's instructions. siRNAs used were: CDC42-1, 5′-TTCAGCAATGCAGACAATTAA-3′; CDC42-2, 5′-CGGAAUAUGUACCGACUGU; JAK2-2, individual ON-TARGETplus J-003146-11-0002; IQGAP1, 5′-UGCCAUGGAUGAGAUUGGA-3′, which were purchased from Dharmacon and for which the Dharmacon nontargeting siRNA 1, 2, or 4 was used as a negative control. JAK2-1 (6235), STAT3-1 (6582), and STAT3-2 (6580) SignalSilence siRNAs were purchased from Cell Signaling Technology, and SignalSilence control siRNA (Cell Signaling Technology, 6508) was used as a negative control.

CDC42 and RAC activation

The PBD fused to GSH *S*-transferase (GST-PBD) was generously provided by Dr. Vijay Shah, Mayo Clinic, and was expressed in *Escherichia coli*. Bacteria were grown to OD 0.5, and then GST-PBD protein expression was induced by isopropyl 1-thio-β-D-galactopyranoside for 3 h at room temperature. The bacteria were lysed by sonication in lysis buffer (50 mM Tris, pH 7.4, 50 mM NaCl, 5 mM $MgCl_2$, 1% Triton X-100, 1 mM DTT, and Complete protease inhibitors (Roche Applied Science)). Following clearance of insoluble material by centrifugation, the supernatant was incubated with GSH-Sepharose (Amersham Biosciences) for 90 min at 4 °C followed by washing with modified lysis buffer (no Triton X-100). Beads were resuspended in lysis buffer and 50% glycerol and stored at 4 °C (32).

For analysis of active CDC42 or RAC1, human pancreatic cancer cells were serum-starved overnight and then treated with IL-6 for the indicated times and dose. The cells were lysed rapidly on ice in lysis buffer (50 mM Tris, pH 7.4, 500 mM NaCl, 5 mM $MgCl_2$, 0.5% IGEPAL, 10% glycerol, and Complete protease inhibitors), vortexed for 5 s, and centrifuged for 2 min at 4 °C. The clarified lysate was incubated with 10 μg of GST-PBD for 10 min at 4 °C. 5% of the volume was retained as the input control. GST-PBD pulldowns and input controls were boiled

ASBMB

with Laemmli buffer, resolved by SDS-PAGE, and immunoblotted for CDC42 or RAC1. Western blots were quantified using a Bio-Rad GelDoc system or ImageJ software. The signal for active CDC42 or RAC1 was normalized to total CDC42 or RAC1 at each time point and then normalized to $t = 0$. Graphed data represent the mean ± S.E. for each condition from at least three independent biological replicates. p values were calculated using a paired, one-tailed Student's t test with the exception of Fig. 2*A* and Figs. S2, *B* and *E*, and 3*A* where a Mann–Whitney one-tailed U test was used due to nonnormal distribution of data. p values less than 0.5 were considered statistically significant differences.

RhoA activation

The RhoA-binding domain of Rhotekin fused to GST, a gift from Dr. Martin Schwartz (Addgene plasmid 15247) (33), was transformed into *E. coli* and purified as described previously (34). Bacteria were cultured to OD 0.8, and then GST-RBD was induced by isopropyl 1-thio-β-D-galactopyranoside for 3 h at room temperature. Bacteria were lysed in ice-cold lysis buffer (50 mM Tris, pH 7.5, 1% Triton X-100, 150 mM NaCl, 5 mM $MgCl_2$, 1 mM DTT, and Complete protease inhibitors), sonicated, and clarified by centrifugation. Clarified lysate was incubated with GSH-Sepharose beads for 60 min at 4 °C and then washed with modified lysis buffer (containing 0.5% Triton X-100). Beads were resuspended in lysis buffer containing 10% glycerol and stored at −80 °C.

To measure RhoA activation, PANC-1 cells were serum-starved overnight in DMEM and then stimulated with IL-6 (50 ng/ml; 5 min). Cells were washed with cold Tris-buffered saline and scraped into lysis buffer (50 mM Tris, pH 7.2, 1% Triton X-100, 0.5% sodium deoxycholate, 0.1% SDS, 500 mM NaCl, 10 mM $MgCl_2$, and Complete protease inhibitors). Lysates were clarified by centrifugation and incubated with GST-RBD beads for 60 min at 4 °C. The beads were washed with (50 mM Tris, pH 7.2, 1% Triton X-100, 150 mM NaCl, 10 mM $MgCl_2$, Complete protease inhibitors) and then boiled with 2× Laemmli sample buffer. 5% of the lysate was used as an input control. GST-RBD pulldowns and input were resolved by SDS-PAGE and immunoblotted for RhoA. The signal for active RhoA was normalized to total RhoA at each time point and then normalized to $t = 0$. Graphed data represent the mean ± S.E. for each condition from three independent biological replicates. p values were calculated using a paired, one-tailed Student's t test.

Immunoprecipitation and immunoblotting

For Western blotting, proteins were resolved by SDS-PAGE, transferred to PVDF (Millipore), blocked in 5% milk (Bio-Rad) or 5% BSA (Sigma), and incubated with primary antibodies overnight (CDC42, BD Transduction Laboratories, 610928; RAC1, clone 23A8, Millipore, 05-389; RhoA, Santa Cruz Biotechnology, sc-418; actin, Sigma, A2066; JAK2, clone D2E12, Cell Signaling Technology, 3230; STAT3, clone D3Z2G, Cell Signaling Technology, 12640; phospho-STAT3, clone D3A7, Cell Signaling Technology, 9145; phospho-ERK, clone 197G2, Cell Signaling Technology, 4377; IQGAP1, Santa Cruz Biotechnology, sc-376021). Secondary antibodies were goat anti-mouse or -rabbit conjugated to horseradish peroxidase (BIOSOURCE International). Chemiluminescence was detected by incubation with SuperSignal Pico or Femto substrates (Thermo Scientific) and exposure to autoradiographic film (HyBlot CL). Western blots were quantified from exposures in the linear range using a Bio-Rad GelDoc system or ImageJ software. Image adjustments were made uniformly across the whole image.

For identification of STAT3-binding partners, PANC-1 cells were transfected with pcDNA3-STAT3, serum-starved overnight in DMEM, and lysed in cytoplasmic fractionation buffer (50 mM Tris, pH 7.4, 150 mM NaCl, 1% IGEPAL, 2 mM EDTA, 1 mM Na_3VO_4, and Complete protease inhibitors). Lysates were incubated on ice for 10 min and centrifuged at 3000 rpm for 15 min at 4 °C. STAT3 was immunoprecipitated from the supernatant using anti-STAT3 rabbit mAb (Cell Signaling Technology, clone D3Z2G, 12640) overnight. The antibody complex was precipitated using 5 mg of Protein A beads (Sigma) prehydrated for 1 h and equilibrated with lysis buffer. Immunoprecipitates were washed three times with lysis buffer and boiled with Laemmli sample buffer. Sample were resolved by SDS-PAGE and silver-stained using the Pierce Silver Stain kit (Thermo Fisher Scientific, Bremen, Germany). Protein identification was performed via an in-gel trypsin digest followed by nano-LC-MS/MS with hybrid orbitrap/linear ion MS using a Thermo Scientific Q-Exactive mass spectrometer (Thermo Fisher Scientific) coupled to a Thermo Ultimate 3000 RSLCnano HPLC system (35). MS/MS samples were analyzed using Mascot (Matrix Science, London, UK; version 2.4.0) and X! Tandem (The Global Proteome Machine; version CYCLONE (2013.09.01)) to search the UniProt January 2017 human protein database based on taxonomy 9606. Scaffold (version Scaffold_4.8.1, Proteome Software Inc., Portland, OR) was used to validate MS/MS-based peptide and protein identifications (36, 37).

For coimmunoprecipitation, cells were lysed on ice in modified Nonidet P-40 lysis buffer (20 mM Tris-HCl, pH 8.0, 200 mM NaCl, 1% IGEPAL, 10% glycerol, 2 mM EDTA, 15 mM NaF, 2 mM Na_3VO_4, and Complete protease inhibitors). STAT3 was immunoprecipitated as described above. Approximately 4% of the lysate was reserved as an input control. Samples were resolved by SDS-PAGE and immunoblotted as described above.

Migration assays

Transwell migration assays were performed using blind well chambers from Neuroprobe (BW200L). Polycarbonate track etch filters with 8-μm pores (Neuroprobe, PFA8) were coated with 0.1% gelatin overnight (Sigma) and then air-dried at room temperature. Pancreatic cancer cells were deprived of serum overnight, then trypsinized, and resuspended in serum-free medium ± IL-6 (50 ng/ml). The lower well contained 10% FBS ± IL-6. Note that IL-6 was maintained in both the upper and lower wells and was not included in the chemotactic gradient. As a positive control, PDGF (30 ng/ml; Peprotech) was included in the lower chamber. For specificity experiments, cells were incubated with blocking antibodies to IL-6 receptor (0.4 μg/ml; Bio-Techne, AF-227 NA), gp-130 (2 μg/ml; Bio-Techne, AF-228 NA), or goat IgG control (2 μg/ml; Santa Cruz Biotechnology). 10×10^5 cells were seeded in the upper well and allowed to migrate for 7 h (PANC-1) or 20 h (CFPAC,

5160-1, and 6741-1). The membranes were removed, cells on both the top and bottom were fixed in formaldehyde, and the nuclei were stained using Hoechst 33342 (Cambrex Bioscience). The membranes were imaged using fluorescence microscopy, and the nuclei on the top and bottom of the filter were scored. At least 10 fields were scored per filter at 40× magnification. For untransfected cells or siRNA experiments, between 436 and 820 cells were scored per filter. CDC42 protein levels were immunoblotted on residual cells from each experiment or on cells transfected in parallel. For CDC42 T17N overexpression experiments, cells were immunostained for myc-CDC42 T17N, and only cells positive for the construct were scored. Between 132 and 215 CDC42 T17N–positive cells were scored per filter. At least three independent biological replicates were performed for each experimental question.

For wound healing assays, cells were grown to high density on gridded glass coverslips and deprived of serum overnight, and then the monolayer was scratched using a plastic pipette tip. Cells were then incubated in the presence or absence of IL-6 (50 ng/ml) in serum-free medium or in medium containing 10% FBS. Phase-contrast photomicrographs were taken of at least three fields per condition after 16 (with 10% FBS) or 24 h (no serum). Images from starting and end points were overlaid in Adobe Photoshop, and iVision software (BioVision Technologies) was used to measure the distance migrated over time.

For cell viability assays, PANC-1 cells were seeded in 96-well plates and treated with IL-6 (50 ng/ml) or EGF (30 ng/ml) for 96 h in DMEM with or without 10% FBS. Cell viability was measured using the CellTiter 96 Aqueous Non-Radioactive Cell Proliferation Assay (Promega).

Immunofluorescence and live-cell imaging

For immunofluorescence, cells were incubated in fixation buffer (0.1 M PIPES, pH 6.9, 1 mM EGTA, 3 mM $MgSO_4$, and 2.5% formaldehyde) for 20 min at 37 °C. The cells were permeabilized in 0.1% Triton X-100 for 2 min and blocked for at least 1e h (5% goat serum, 5% glycerol, and 0.04% sodium azide, pH 7.2). For STAT3 staining, cells were permeabilized in cold 100% methanol at −20 °C for 10 min according to the antibody instructions. The following primary antibodies were used for immunofluorescence: myc tag, clone 71D10, Cell Signaling Technology, 2278; STAT3, clone D3Z2G, Cell Signaling Technology, 12640; IQGAP1, Santa Cruz Biotechnology, sc-376021. Secondary antibodies were goat anti-mouse/rabbit conjugated to the appropriate fluorophores (Alexa Fluor 488, Fluor Alexa 532, and Cy5). Coverslips were mounted on slides using Prolong Gold (Molecular Probes). Images were acquired using a Zeiss Axiovert 35 epifluorescence microscope using a 40× objective for transwell migration assays, a 10× objective for wound healing assays, or a 63× oil objective for STAT3 localization, and a Hamamatsu OrcaII camera with either iVision or Zeiss software. Images were processed using Adobe Photoshop software, and any adjustments were applied uniformly to the entire image.

Live-cell imaging of GFP-actin in PANC-1 cells was performed on a Zeiss LSM 780 confocal microscope with a 63× objective lens in a heated chamber at 37 °C in 5% CO_2. PANC-1 cells were starved overnight in serum-free DMEM, and the medium was replaced before imaging. Images were acquired every 20 s for 10 min, and then 200 μl of IL-6 diluted in DMEM was added to 1.8 ml of DMEM in imaging dishes to achieve a final concentration of 50 ng/ml IL-6. Imaging was continued for 30 min to observe formation of filopodia. Movies were processed using NIH ImageJ software. The number of filopodia was quantified using the ImageJ program FiloQuant (17).

Author contributions—G. L. R. conceptualization; G. L. R. formal analysis; G. L. R. supervision; G. L. R. and M. A. M. funding acquisition; G. L. R. and K. M. B. investigation; G. L. R. and K. M. B. methodology; G. L. R. and K. M. B. writing-original draft; G. L. R., K. M. B., and M. A. M. writing-review and editing; M. A. M. resources.

Acknowledgments—We are grateful to Dr. Micah Schott and members of the McNiven laboratory for technical support, helpful suggestions, and critical reading of the manuscript. We acknowledge the Mayo Clinic Medical Genome Facility-Proteomics Core and its supporting grant, National Institutes of Health NCI Cancer Center Support Grant 5P30 CA15083-43C1.

References

1. Siegel, R. L., Miller, K. D., and Jemal, A. (2017) Cancer Statistics, 2017. *CA Cancer J. Clin.* **67,** 7–30 CrossRef Medline
2. Rhim, A. D., Mirek, E. T., Aiello, N. M., Maitra, A., Bailey, J. M., McAllister, F., Reichert, M., Beatty, G. L., Rustgi, A. K., Vonderheide, R. H., Leach, S. D., and Stanger, B. Z. (2012) EMT and dissemination precede pancreatic tumor formation. *Cell* **148,** 349–361 CrossRef Medline
3. Grivennikov, S. I., Greten, F. R., and Karin, M. (2010) Immunity, inflammation, and cancer. *Cell* **140,** 883–899 CrossRef Medline
4. Öhlund, D., Handly-Santana, A., Biffi, G., Elyada, E., Almeida, A. S., Ponz-Sarvise, M., Corbo, V., Oni, T. E., Hearn, S. A., Lee, E. J., Chio, I. I., Hwang, C. I., Tiriac, H., Baker, L. A., Engle, D. D., *et al.* (2017) Distinct populations of inflammatory fibroblasts and myofibroblasts in pancreatic cancer. *J. Exp. Med.* **214,** 579–596 CrossRef Medline
5. Zhang, Y., Yan, W., Collins, M. A., Bednar, F., Rakshit, S., Zetter, B. R., Stanger, B. Z., Chung, I., Rhim, A. D., and di Magliano, M. P. (2013) Interleukin-6 is required for pancreatic cancer progression by promoting MAPK signaling activation and oxidative stress resistance. *Cancer Res.* **73,** 6359–6374 CrossRef Medline
6. Lesina, M., Kurkowski, M. U., Ludes, K., Rose-John, S., Treiber, M., Klöppel, G., Yoshimura, A., Reindl, W., Sipos, B., Akira, S., Schmid, R. M., and Algül, H. (2011) Stat3/Socs3 activation by IL-6 transsignaling promotes progression of pancreatic intraepithelial neoplasia and development of pancreatic cancer. *Cancer Cell* **19,** 456–469 CrossRef Medline
7. Nagathihalli, N. S., Castellanos, J. A., VanSaun, M. N., Dai, X., Ambrose, M., Guo, Q., Xiong, Y., and Merchant, N. B. (2016) Pancreatic stellate cell secreted IL-6 stimulates STAT3 dependent invasiveness of pancreatic intraepithelial neoplasia and cancer cells. *Oncotarget* **7,** 65982–65992 CrossRef Medline
8. Corcoran, R. B., Contino, G., Deshpande, V., Tzatsos, A., Conrad, C., Benes, C. H., Levy, D. E., Settleman, J., Engelman, J. A., and Bardeesy, N. (2011) STAT3 plays a critical role in KRAS-induced pancreatic tumorigenesis. *Cancer Res.* **71,** 5020–5029 CrossRef Medline
9. Taniguchi, K., and Karin, M. (2014) IL-6 and related cytokines as the critical lynchpins between inflammation and cancer. *Semin. Immunol.* **26,** 54–74 CrossRef Medline
10. Fukuda, A., Wang, S. C., Morris, J. P., 4th, Folias, A. E., Liou, A., Kim, G. E., Akira, S., Boucher, K. M., Firpo, M. A., Mulvihill, S. J., and Hebrok, M. (2011) Stat3 and MMP7 contribute to pancreatic ductal adenocarcinoma initiation and progression. *Cancer Cell* **19,** 441–455 CrossRef Medline
11. Huang, C., Yang, G., Jiang, T., Zhu, G., Li, H., and Qiu, Z. (2011) The effects and mechanisms of blockage of STAT3 signaling pathway on IL-6

inducing EMT in human pancreatic cancer cells *in vitro*. *Neoplasma* **58,** 396–405 CrossRef Medline

12. Tam, W. L., and Weinberg, R. A. (2013) The epigenetics of epithelial-mesenchymal plasticity in cancer. *Nat. Med.* **19,** 1438–1449 CrossRef Medline
13. Fischer, K. R., Durrans, A., Lee, S., Sheng, J., Li, F., Wong, S. T., Choi, H., El Rayes, T., Ryu, S., Troeger, J., Schwabe, R. F., Vahdat, L. T., Altorki, N. K., Mittal, V., and Gao, D. (2015) Epithelial-to-mesenchymal transition is not required for lung metastasis but contributes to chemoresistance. *Nature* **527,** 472–476 CrossRef Medline
14. Zheng, X., Carstens, J. L., Kim, J., Scheible, M., Kaye, J., Sugimoto, H., Wu, C. C., LeBleu, V. S., and Kalluri, R. (2015) Epithelial-to-mesenchymal transition is dispensable for metastasis but induces chemoresistance in pancreatic cancer. *Nature* **527,** 525–530 CrossRef Medline
15. Ridley, A. J. (2011) Life at the leading edge. *Cell* **145,** 1012–1022 CrossRef Medline
16. Pal, K., Pletnev, A. A., Dutta, S. K., Wang, E., Zhao, R., Baral, A., Yadav, V. K., Aggarwal, S., Krishnaswamy, S., Alkharfy, K. M., Chowdhury, S., Spaller, M. R., and Mukhopadhyay, D. (2014) Inhibition of endoglin-GIPC interaction inhibits pancreatic cancer cell growth. *Mol. Cancer Ther.* **13,** 2264–2275 CrossRef Medline
17. Jacquemet, G., Paatero, I., Carisey, A. F., Padzik, A., Orange, J. S., Hamidi, H., and Ivaska, J. (2017) FiloQuant reveals increased filopodia density during breast cancer progression. *J. Cell Biol.* **216,** 3387–3403 CrossRef Medline
18. Bartolomé, R. A., Molina-Ortiz, I., Samaniego, R., Sánchez-Mateos, P., Bustelo, X. R., and Teixidó, J. (2006) Activation of Vav/Rho GTPase signaling by CXCL12 controls membrane-type matrix metalloproteinase-dependent melanoma cell invasion. *Cancer Res.* **66,** 248–258 CrossRef Medline
19. Matsuguchi, T., Inhorn, R. C., Carlesso, N., Xu, G., Druker, B., and Griffin, J. D. (1995) Tyrosine phosphorylation of p95Vav in myeloid cells is regulated by GM-CSF, IL-3 and steel factor and is constitutively increased by p210BCR/ABL. *EMBO J.* **14,** 257–265 Medline
20. Siddiquee, K., Zhang, S., Guida, W. C., Blaskovich, M. A., Greedy, B., Lawrence, H. R., Yip, M. L., Jove, R., McLaughlin, M. M., Lawrence, N. J., Sebti, S. M., and Turkson, J. (2007) Selective chemical probe inhibitor of Stat3, identified through structure-based virtual screening, induces antitumor activity. *Proc. Natl. Acad. Sci. U.S.A.* **104,** 7391–7396 CrossRef Medline
21. Kaptein, A., Paillard, V., and Saunders, M. (1996) Dominant negative stat3 mutant inhibits interleukin-6-induced Jak-STAT signal transduction. *J. Biol. Chem.* **271,** 5961–5964 CrossRef Medline
22. Selvaraj, B. T., Frank, N., Bender, F. L., Asan, E., and Sendtner, M. (2012) Local axonal function of STAT3 rescues axon degeneration in the pmn model of motoneuron disease. *J. Cell Biol.* **199,** 437–451 CrossRef Medline
23. Zhou, Z., Gushiken, F. C., Bolgiano, D., Salsbery, B. J., Aghakasiri, N., Jing, N., Wu, X., Vijayan, K. V., Rumbaut, R. E., Adachi, R., Lopez, J. A., and Dong, J. F. (2013) Signal transducer and activator of transcription 3 (STAT3) regulates collagen-induced platelet aggregation independently of its transcription factor activity. *Circulation* **127,** 476–485 CrossRef Medline
24. Teng, T. S., Lin, B., Manser, E., Ng, D. C., and Cao, X. (2009) Stat3 promotes directional cell migration by regulating Rac1 activity via its activator βPIX. *J. Cell Sci.* **122,** 4150–4159 CrossRef Medline
25. Swart-Mataraza, J. M., Li, Z., and Sacks, D. B. (2002) IQGAP1 is a component of CDC42 signaling to the cytoskeleton. *J. Biol. Chem.* **277,** 24753–24763 CrossRef Medline
26. Smith, J. M., Hedman, A. C., and Sacks, D. B. (2015) IQGAPs choreograph cellular signaling from the membrane to the nucleus. *Trends Cell Biol.* **25,** 171–184 CrossRef Medline
27. Watanabe, T., Wang, S., and Kaibuchi, K. (2015) IQGAPs as key regulators of actin-cytoskeleton dynamics. *Cell Struct. Funct.* **40,** 69–77 CrossRef Medline
28. Socoro-Yuste, N., Dagher, M. C., Gonzalez De Peredo, A., Mondet, J., Zaccaria, A., Roux Dalvai, F., Plo, I., Cahn, J. Y., and Mossuz, P. (2016) Ph(−) myeloproliferative neoplasm red blood cells display deregulation of IQGAP1-Rho GTPase signaling depending on CALR/JAK2 status. *Biochim. Biophys. Acta* **1863,** 2758–2765 CrossRef Medline
29. Toffali, L., Montresor, A., Mirenda, M., Scita, G., and Laudanna, C. (2017) SOS1, ARHGEF1, and DOCK2 rho-GEFs Mediate JAK-Dependent LFA-1 Activation by Chemokines. *J. Immunol.* **198,** 708–717 CrossRef Medline
30. Kim, J. H., Yoon, M. S., and Chen, J. (2009) Signal transducer and activator of transcription 3 (STAT3) mediates amino acid inhibition of insulin signaling through serine 727 phosphorylation. *J. Biol. Chem.* **284,** 35425–35432 CrossRef Medline
31. Choidas, A., Jungbluth, A., Sechi, A., Murphy, J., Ullrich, A., and Marriott, G. (1998) The suitability and application of a GFP-actin fusion protein for long-term imaging of the organization and dynamics of the cytoskeleton in mammalian cells. *Eur. J. Cell Biol.* **77,** 81–90 CrossRef Medline
32. Wittchen, E. S., and Burridge, K. (2008) Analysis of low molecular weight GTPase activity in endothelial cell cultures. *Methods Enzymol.* **443,** 285–298 CrossRef Medline
33. Ren, X. D., Kiosses, W. B., and Schwartz, M. A. (1999) Regulation of the small GTP-binding protein Rho by cell adhesion and the cytoskeleton. *EMBO J.* **18,** 578–585 CrossRef Medline
34. Ren, X. D., and Schwartz, M. A. (2000) Determination of GTP loading on Rho. *Methods Enzymol.* **325,** 264–272 CrossRef Medline
35. Michalski, A., Damoc, E., Hauschild, J. P., Lange, O., Wieghaus, A., Makarov, A., Nagaraj, N., Cox, J., Mann, M., and Horning, S. (2011) Mass spectrometry-based proteomics using Q Exactive, a high-performance benchtop quadrupole Orbitrap mass spectrometer. *Mol. Cell. Proteomics* **10,** CrossRef Medline
36. Nesvizhskii, A. I., Keller, A., Kolker, E., and Aebersold, R. (2003) A statistical model for identifying proteins by tandem mass spectrometry. *Anal. Chem.* **75,** 4646–4658 CrossRef Medline
37. Keller, A., Nesvizhskii, A. I., Kolker, E., and Aebersold, R. (2002) Empirical statistical model to estimate the accuracy of peptide identifications made by MS/MS and database search. *Anal. Chem.* **74,** 5383–5392 CrossRef Medline